Prostate Tissue Characterization Using TRUS Image Spectral Features

S.S. Mohamed[1], A.M.Youssef[2], E.F El-Saadany[1], and M.M.A. Salama[1]

[1] Department of Electrical and Computer Engineering,
University of Waterloo, Ontario, Canada
{smohamed, ehab, msalama}@hivolt.uwaterloo.ca
[2] Concordia Institute for Information Systems Engineering,
Concordia University, Montréal, Quebec, Canada
youssef@ciise.concordia.ca

Abstract. In this paper focuses on extracting and analyzing spectral features from Trans-Rectal Ultra-Sound (TRUS) images for prostate tissue characterization. The information of the images' frequency domain features and spatial domain features are used to achieve an accurate Region of Interest (ROI) identification. In particular, each image is divided into ROIs by the use of Gabor filters, a crucial stage, where the image is segmented according to the frequency response of the image pixels. Further, pixels with a similar response to the same filter are assigned to the same region to form a ROI. The radiologist's experience is also integrated into the algorithm to identify the highly suspected ROIs.

Next, for each ROI, different spectral feature sets are constructed. One set includes the power spectrum wedge and ring energies. The other sets are constructed using geometrical features extracted from the Power Spectrum Density (PSD). In particular, the estimated PSD in these sets is divided into two segments. Polynomial interpolation is used for the first segment and the obtained polynomial coefficients are used as features. The second segment is approximated by a straight line and the slope, the Y intercept as well as the first maximum reached by the PSD are considered as features.

A classifier-based feature selection algorithm using CLONALG, a recently proposed optimization technique developed on the basis of clonal selection of the Artificial Immune System (AIS), is adopted and used to select an optimal subset from the above extracted features. Using different PSD estimation techniques, the obtained accuracy ranges from 72.2% to 93.75% using a Support Vector Machine classifier.

1 Introduction

The Prostate is a male gland that is located around the urethra. The Prostate is considered as three glandular structures which are the peripheral zone, the central zone and the transition zone [1]. Prostate Cancer is the second most diagnosed malignancy in men over the age of fifty [2]. Symptoms due to carcinoma of the prostate are generally absent until extensive local growth or metastases develop. Risk of metastasis dramatically increases once the tumor has extended beyond the prostate

A. Campilho and M. Kamel (Eds.): ICIAR 2006, LNCS 4142, pp. 589 – 601, 2006.

[3]. Since Prostate cancer is better curable at an early stage, early detection is highly crucial [4]. Prostate-specific antigen (PSA) and Digital Rectal Exams (DRE) are considered the typical assessments for screening individuals for prostate cancer [2]. The combination of these two diagnostic techniques has improved the diagnostic path by allowing for an earlier detection of tumors [5]. However, PSA has limited specificity in that it is not a tumor marker, but its value can increase due to different effects such as prostate volume increase, benign prostatic hyperplasia (BPH) and Prostatitis [6]. Another diagnostic method is the determination of the prostate volume. The prostate volume is a crucial parameter in the diagnosis and management of both benign and malignant prostatic diseases. This is usually achieved by using either CT imaging system, MRI imaging or TRUS imaging system. It was shown in [7] that the volume obtained using TRUS is more accurate than the volume obtained using CT. In a comparison between the TRUS imaging, the MRI imaging modalities and the DRE, the MRI slightly outperformed the TRUS in prostate cancer staging; however, the DRE results in far less staging ability than the TRUS [8]. From the previous discussion as well as the affordable price and the simplicity it is clear that using the TRUS imaging modality is the most favorable. Moreover**,** the internal architecture of the prostate can be detailed by TRUS, and the procedure allows an accurate measurement of prostate volume. Therefore, TRUS has become the most frequently used prostate imaging modality**.** Prostate carcinoma has a characteristic hypo-echoic pattern which is sometimes distinct from the normal echo pattern of the peripheral portion of the prostate. However, TRUS is still lacking sufficient sensitivity and specificity to support its use for routine screening for prostate cancer. In men with an abnormality of either DRE of the prostate or serum PSA, TRUS is useful for directing prostate biopsy. This is usually achieved with the aid of an expert radiologist [9]. The existing diagnostic methods such as Digital Rectal Exam (DRE), TRUS imaging system, PSA measure and prostate volume have proven to be insufficient. For instance, both DRE and TRUS are highly dependent on the skills of the conducting physician and radiologist. Experienced doctors achieve more accurate prediction rates than inexperienced doctors due to the fact that prior knowledge is a must to the success of applying these methods. This is the main motivation for designing a new system in which experienced radiologists knowledge can provide feedback to supplement the knowledge of newer radiologists in decision making. In other words, our objective is improving the Computer Aided Diagnosis (CAD) techniques in order to assist the radiologists' decision making process.

When using CAD as a tool in ultrasound imaging, features are constructed from the echoes after the echo processing for image tissue typing. Such features can include either the statistical characteristics of the grey level distribution in the image [10,11,12] or the spectral features from the RF- echo signals before image formation [13,14].

Spectral methods proved excellent recognition ability when applied to the RF data, i.e., before the formation of the TRUS image [13,14]. Unfortunately, the RF data may not be available for many researchers. Hence, they cannot benefit from this powerful method. In this work, we explore the application of different spectral methods to the TRUS images.

The proposed system is composed of four main stages. The first stage is identifying the high risk ROIs in the image. In the second stage, different spectral features are constructed from the ROIs. In the third stage, a classifier-dependent feature selection algorithm using the CLONALG, a recently proposed optimization technique developed

on the basis of clonal selection of the Artificial Immune System (AIS), is adopted and used to select an optimal subset from the above extracted features. Finally, SVM is used for testing the system accuracy using the selected feature sets. The system block diagram is shown in Figure 1.

The paper is organized as follows: Section 2 outlines the ROI identification algorithm, Section 3 covers the wedge and ring feature construction method and a brief survey of the different power spectrum estimation methods used in this work. Section 4 highlights the clonal selection algorithm and its application for feature selection. Section 5 summarizes the SVM classification method. The results and discussion are provided in section 6, and finally, the conclusion is given in Section 7.

2 TRUS Images ROI Identification

The images used in our investigation are obtained from the University of Western Ontario, Canada, and are derived from the Aloka 2000 ultrasound machine using a broadband 7MHz linear transducer, and a field of view of approximately 6 cm. The results reported in this paper are based on a set of 33 professionally identified TRUS images, where suspected cancer regions are highlighted by an expert radiologist.

Classical CAD techniques rely on the radiologist to mark the ROIs on the ultrasound image. Alternatively, the whole ultrasound image is divided into small squares and each one of these squares is treated as a possible ROI. In this work, in order to assist the radiologist and produce a more accurate result, an automated ROI identification algorithm based on Gabor multi-resolution analysis is implemented.

The Gabor multi-resolution analysis has been used for a long time in the image segmentation field [15]. It shows promising results for TRUS image texture segmentation [16]. In this work, the Gabor multi-resolution analysis is applied to the prostate TRUS image in order to identify the ROIs. The main advantage of this method is that no prior image assessment is required from the radiologist. Moreover, the proposed algorithm is fast and efficient. The algorithm uses both the frequency domain information, as well as the spatial domain information from the image. This process is achieved by applying the Gabor multi-resolution analysis that is capable of segmenting the image according to the frequency response of the pixels. The pixels that have similar response are assigned to the same cluster. This process segments the TRUS image into several ROIs. The Gabor function is chosen for its high localization in both the frequency domain, as well as the spatial domain.

By integrating the expert radiologist's knowledge into the algorithm, only a subset of the resulting segments is identified as ROIs. This is achieved by incorporating some observations regarding some statistics of the radiologist marked regions such as length and frequency level. These criteria were set into the algorithm to best mimic the radiologist's decision.

A sample of the results of this ROI identification method is shown in Figures 2. The images on the left side show the ROIs identified and marked by an expert radiologist. The left side shows the ROIs identified by the proposed algorithm.

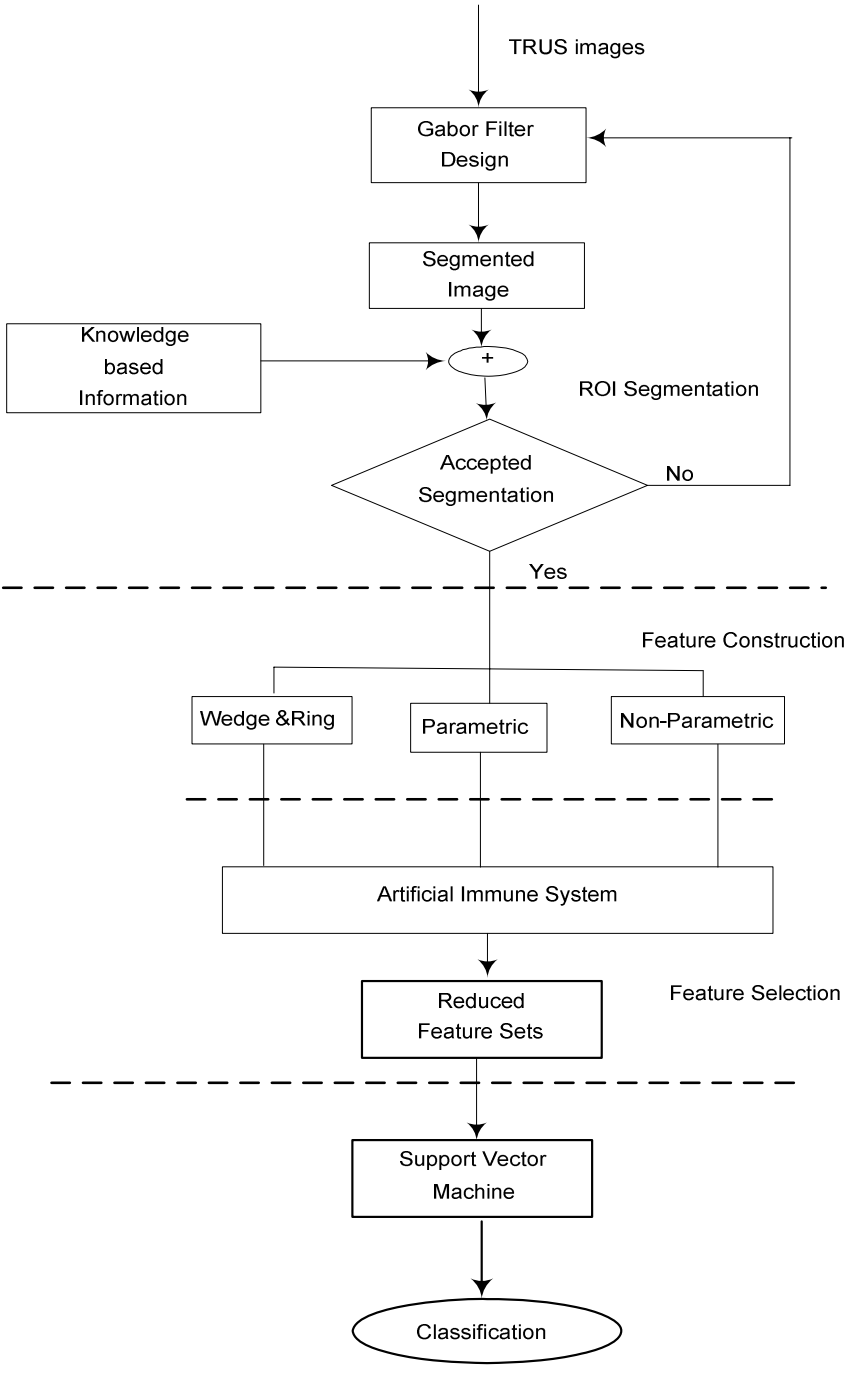

Fig. 1. Prostate cancer diagnosis from TRUS images

3 ROI Power Spectrum Density Estimation Methods

Different spectral features from the RF-echo signals, i.e., before the ultrasound image formation, have been used successfully for cancer diagnosis. Unfortunately, the RF signal may not be available to most researchers. In this work, we investigate the application of different spectral methods to the TRUS images. The methods used are briefly surveyed in this section.

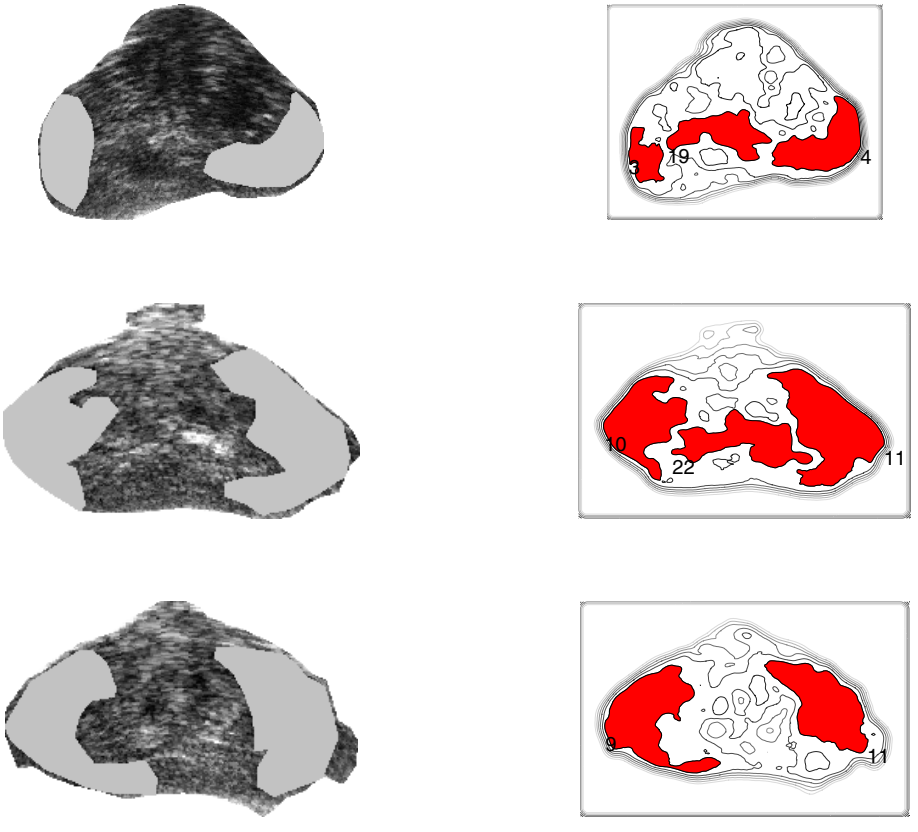

Fig. 2. Three different TRUS professionally segmented images and their corresponding ROIs

3.1 Wedge and Ring Method

The Fourier transform in its discrete form is the most widely used transform for the analysis of textured scenes [17]. Information is provided on textural content by extracting features from the Fourier power spectrum, as it represents the strength of each spatial frequency. The transformation of textured images into the Fourier domain provides a more brief form of representing the textural information within the image. The textural properties revealed from the power spectrum are coarseness (periodicity)

and directionality. Texture directionality is almost preserved in the power spectrum, which allows directional and non-directional components of the texture to be distinguished. Therefore, conclusions about the shape properties of a texture can be defined [17,18]. Coarse textures have power spectrum values concentrated near the origin, while fine textures have more high frequency components, hence; have a more spread out spectrum. These observations result in the features extracted in the Fourier domain ring and wedge filters. These filters were introduced in [19] and were used for image segmentation in [20] where it was compared to other image features. The power is measured between rings of inner radius r_1 and outer radius r_2. The directionality of the image texture is represented by the average power over wedge-shaped regions centered at the origin of the power spectrum.

This method is summarized as follows. For any spatial position (x, y) on the image, there is a function $f(x, y)$ representing the grey scale level of the TRUS image. Thus, the 2D Fourier-transform pair for an image of width M_s and height N_s has the form,

$$\Im\{f(x,y)\} = F(u,v) = \frac{1}{M_s N_s} \sum_{x=0}^{M_s-1} \sum_{y=0}^{N_s-1} f(x,y) \exp\left[- j2\pi \left(\frac{ux}{M_s} + \frac{vy}{N_s} \right) \right]$$

for $u, x = 0,1,2,\cdots, M_s - 1$ and $v, y = 0,1,2,\cdots, N_s - 1$

For deterministic signals, the square of the magnitude of the Fourier spectrum is referred to as the power spectrum of f. Let $P(u,v) = |\Im(u,v)|^2$ and let $P_{r\phi}(r, \phi)$ denote the corresponding function in the spherical coordinates, i.e., with $r = \sqrt{u^2 + v^2}$ and $\phi = \tan^{-1}(\frac{v}{y})$.

Then the power contained in a ring centered at the origin having inner and outer radii of r_1 and r_2 respectively, is given by $\sum_{r=r1}^{r2} \sum_{\phi=0}^{\pi} P_{r\phi}(r, \phi)$. Similarly, the power contained in a wedge of radius r and bounded between ϕ_1 and ϕ_2 is given by $\sum_{r=0}^{r} \sum_{\phi=\phi_1}^{\phi_2} P_{r\phi}(r, \phi)$.

This method is applied to the ROIs of the TRUS image and the normalized energy (per pixel) content in ten wedges and ten rings is calculated. One clear weakness of this method is that rings and wedges geometry do not match the irregular nature of the ROIs in the TRUS images.

For the methods described throughout the rest of this paper, the pixels within each ROI are aligned to form a 1-Dimessional signal and the PSD is calculated for this signal. Then a feature set is constructed using geometrical features extracted from the PSD. In particular, the estimated PSD in this set is divided into two segments based on visual inspection of the PSD graph. Polynomial interpolation is used for the first segment and the obtained polynomial coefficients are used as features. The second

segment is approximated by a straight line and the slope, the Y intercept as well as the first maximum reached by the PSD are considered as features.

The used PSD estimation methods have been explained thoroughly in literature [21, 22]. These methods can be categorized into two main categories, namely the parametric and the non-parametric methods.

3.2 Parametric Power Density Estimation Methods

The data is modeled as the output of a linear system driven by white noise [21, 22], and the parameters of this linear system are estimated. The most commonly used model is the *all pole* model, whose output for a white noise input is an AR process. Therefore, these methods are referred to as AR methods for spectral estimation. From the mode and the estimated parameters the PSD can be estimated. The AR methods tend to adequately describe peaky spectral data such as speech signals. Due to the fact that ultrasound images have high frequency changes, hence AR methods are selected to describe the TRUS images' data. The data is estimated by linear combination of past values (forward prediction) and/or future values (backward prediction). The unknown coefficients are found by minimizing the errors between the predicted values and the original data [21]. All AR models give a PSD estimate given by

$$P_{xx}(f) = \frac{\hat{\sigma}^2}{\left|1 + \sum_{k=1}^{p} \hat{a}_p(k) e^{-2\lambda fk}\right|^2}$$

Where $\hat{a}_p(k)$ are the estimates of the AR parameters and $\hat{\sigma}^2$ is the estimated minimum mean square value for the p^{th} order predictor.

Yule-Walker AR Method. This method is also named as the autocorrelation method. This method estimates the PSD of the input by fitting an autoregressive (AR) model to the windowed input data by minimizing the forward prediction error in the least squares sense [21]. This formulation leads to the Yule-Walker equations, which are solved by Levinson-Durbin recursion where a biased form of the autocorrelation estimate is used which ensures that the autocorrelation matrix is positive definite. Therefore the matrix is invertible and solution is guaranteed to exist. The AR model parameters are obtained by solving the following Yule-Walker equations

$$\begin{bmatrix} \gamma_{xx}(0) & \gamma_{xx}(-1) & \vdots & \gamma_{xx}(-p+1) \\ \gamma_{xx}(1) & \gamma_{xx}(0) & \vdots & \gamma_{xx}(-p+2) \\ \vdots & \vdots & \vdots & \vdots \\ \gamma_{xx}(p-1) & \gamma_{xx}(p-2) & \vdots & \gamma_{xx}(0) \end{bmatrix} \begin{bmatrix} a_1 \\ a_2 \\ \vdots \\ a_p \end{bmatrix} = -\begin{bmatrix} \gamma_{xx}(1) \\ \gamma_{xx}(2) \\ \vdots \\ \gamma_{xx}(p) \end{bmatrix}, \text{ where } \gamma_{xx}(m)$$

represent the autocorrelation sequence that is estimated from the data by

$$\gamma_{xx}(m) = \frac{1}{N} \sum_{n=0}^{N-m-1} x^*(n) x(n+m)$$

The estimated minimum mean square value for the p^{th} order predictor is given by

$$\hat{\sigma}^2 = \hat{E}_p^f = \gamma_{xx}(0)\prod_{k=1}^{p}(1-|\hat{a}_k(k)|^2)$$

Burg Method. This method estimates the AR parameters using an order recursive least square lattice method, based on minimizing the forward and backward errors in linear predictors, such that the AR parameters satisfy the Levinson-Durbin recursion. The details of the error prediction are given in [21,23]. This method results in high frequency resolution compared to the Yule-Walker method. It also yields to a stable AR model. The main disadvantage of this method is that it introduces spurious peaks for high order models.

Modified Covariance Method (MCM). The covariance method for AR spectral estimation is based on minimizing the forward prediction error. While, the modified covariance method is based on minimizing the forward and backward prediction errors not constrained by satisfying the Levinson-Durbin recursion. It is shown in [15] that the MCM performs better than the Burg AR model for signals and it is shown in [24] that the modified covariance method performs better than the non-parametric periodogram method for the radar backscatter signals.

3.3 Non-parametric Power Density Estimation Methods

The non-parametric methods tend to estimate the PSD from the observed signal directly. Three different non-parametric methods are used in this work. Further details about these methods can be found in [21].

Modified Periodogram. One way of estimating the power spectrum of a signal is to simply find the discrete-time Fourier transform of the samples of the process and take the magnitude squared of the result. This estimate is called the periodogram. The modified periodogram windows the signal prior to computing the Fourier transform in order to smooth the edges of the signal. This has the effect of reducing the height of the side-lobes or spectral leakage. This phenomenon gives rise to the analysis of side-lobes as spurious frequencies introduced into the signal by the abrupt truncation that occurs when a rectangular window is used. For nonrectangular windows, the end points of the truncated signal are attenuated smoothly, and hence the spurious frequencies introduced are much less severe. On the other hand, nonrectangular windows also broaden the main lobe, which results in a net reduction of resolution. In this work a Hamming window is used.

Welch' Method. Some modifications are applied to the classic periodogram method that allowed overlapping data segments as well as windowing the data segments prior to computing the periodogram. A Hamming window with an overlap of 50% is used in this work.

Multi Taper Method (MTM). The MTM method uses linear or nonlinear combinations of modified periodograms to estimate the PSD. These periodograms are computed using a sequence of orthogonal tapers [22]. Thompson's *multitaper method* (MTM) builds an improved PSD estimate. Instead of using filters that are rectangular

windows as in the periodogram method, the MTM method uses a bank of optimal band-pass filters to compute the estimate. These optimal filters are derived from a set of sequences known as Discrete Prolate Spheroidal Sequences (DPSS) [25]. In addition, the MTM method provides a parameter that could balance the variance and resolution. This parameter is given by the time-bandwidth product, $N\times W$ and it is directly related to the number of tapers used to compute the spectrum. There are always $2N\times W$-1 tapers used to form the estimate. This means that, as $N\times W$ increases, there are more estimates of the power spectrum, and the variance of the estimate decreases. However, the bandwidth of each taper is also proportional to $N\times W$, so as $N\times W$ increases, each estimate exhibits more spectral leakage (i.e., wider peaks) and the overall spectral estimate is more biased.

4 Feature Selection

The output of the spectral feature construction algorithms is a group of feature sets. The parametric and non-parametric methods produce feature sets that are composed of the polynomial coefficients as well as the Y-intercept, slope and the first peak. It is expected that some of these constructed features may not be influential and might carry redundant information which may confuse the classifier. Thus, feature selection and dimensionality reduction is a crucial step to get the best out of the constructed features. While exhaustive search guarantees the global optimal feature subset, its complexity grows exponentially with the dimension of the feature space, which causes this approach to be impractical even for medium number of features.

Artificial Immune Systems (AIS) [27] are computer algorithms inspired by the principles and processes of the vertebrates' immune system. The algorithms exploit the immune system's characteristics of learning and memory to solve a problem. Artificial immune algorithms can be broadly categorized into three subgroups: those using the clonal selection theory, those using negative selection and those using the immune network theory as their main inspiration.

In this work, CLONALG [26], a recently proposed optimization technique developed on the basis of clonal selection of the AIS, is adopted and used to select an optimal subset from the above extracted features. The set of selected features selected by our algorithm is classifier dependant (SVM is used in this work). This means that different possible feature subsets are examined by the algorithm and the classifier performance is tested for each subset and finally the best discriminatory feature subset is chosen by the algorithm. The CLONALG can be summarized as follows:

1. Randomly initialize a population of individuals (M). Each individual corresponds to a binary vector of length equal to the total number of features in the feature set under consideration. The 1's positions denote the set of features selected by this particular individual.
2. The affinity of each individuals is defined as the recognition accuracy corresponding to the features selected by this individual using a pre-specified classifier (in this work, we use Support Vector Machine classifier.)
3. Select the n best highest affinity elements of M and generate copies of these individuals proportionally to their affinity.

4. Mutate all these copies with a rate proportional to their affinity with the input pattern: the higher the affinity, the smaller the mutation rate.
5. Add these mutated individuals to the population *M* and reselect m of these maturated individuals to be kept as memories of the systems.
6. Repeat steps 2 to 5 until a certain criterion is reached (in this work, we fixed the number of iterations).

When the algorithm terminates, it reports the best individual and its affinity, i.e., the accuracy of the classifier when using only the subset of features corresponding to this individual. The above feature selection algorithm was applied to each constructed feature set as well as to all the features combined together.

5 Classification

SVMs are found to be an influential methodology for solving a non-linear classification problem [28] such as the one described in this paper. SVMs has been introduced within the framework of statistical learning theory and structural risk minimization, depending mainly on pre-processing the data to represent patterns in a higher dimensionality space, usually much higher than the original feature space. This is achieved with a suitable non-linear mapping to a sufficiently high dimension. The data from two classes are consistently separated by a hyper-plane. For further information about the SVMs, the reader is referred to [28]. After the best representative feature subset is chosen from each of the available feature sets, each of the selected spectral feature subsets are examined using a SVM classifier. Moreover, all the spectral feature sets that are extracted using all the features above are combined to form one set, which is then reduced using the AIS and tested using the SVMs classifier.

6 Results

A set of 108 regions was used in this study where 90 regions were used as training set and a set of 18 regions was used as the test set. The following parameters are used to evaluate these features:

Accuracy: 1.0 - probability of misclassification
False Negative: probability of classifying a cancerous prostate as a normal prostate.
False Positive: probability of classifying a cancerous prostate as a normal prostate.
Sensitivity: 1.0 - false negative rate
Specificity: 1.0 - false positive rate

Specificity, sensitivity and accuracy are the measures used to test different feature sets applied in this work. The obtained results are shown in Table 1.

It is clear from the results that the wedge and ring filters possess the least accuracy. As mentioned before, this can be explained by the irregular nature of the ROIs. This also proves that dealing with the regions' pixels as individual data points and treating it as a signal is more appropriate for this application. The modified periodogram

method obtained the least accuracy among the PSD estimation techniques and this can be explained by the effect of spectral leakage that occurs for short data sets. Further, the Hamming windows broaden the main lobe, which results in a net reduction of resolution. Moreover, the variance does not tend to zero as the data length tends to infinity. In other words, the periodogram is not a consistent estimator of the PSD especially for short data sets. The Welch's method obtained good results as it tends to decrease the variance of the estimate relative to the periodogram estimate. Although overlap between segments tends to introduce redundant information, this effect is diminished by the use of a Hamming window, which reduces the importance given to the end samples of segments. In the parametric methods, as expected, the modified covariance method obtained the best results. Naturally, combining all the features extracted from the different PSD estimation methods produced the best results as the information from each data set complements each other.

Table 1. Classification results using the constructed feature sets

Input to the feature selection algorithm	% Sensitivity	% Specificity	% Accuracy
Wedge & Ring	66.7	75	72.2
Periodogram	66.67	83.33	77.7
Multi Taper	66.67	91.6	83.3
Welch's	83.3	91.6	88.89
Yule-Walker features	83.3	83.3	83.3
Burg features	83.3	83.3	83.3
Modified Covariance	83.3	91.6	88.89
All Estimated Spectral Features	83.3	100	93.75

7 Conclusions

Using spectral features from TRUS images, we introduced a novel system for Prostate Tissue Characterization. One of the main advantages of the proposed system is the integration of the expert radiologist's knowledge into the algorithm to identify the suspicious ROIs which are further analyzed using spectral features. The proposed system mimics the expert radiologist in detecting possible cancerous regions with high degree of accuracy. Different spectral feature sets were examined. When combining all the estimated PSD features, and using the CLONALG as a feature selection algorithm, SVMs classifier achieved a classification accuracy of 93.75%.

References

1. McNeal, J.E.: Normal and pathologic anatomy of prostate. Urology. 1981 March17:11-16.
2. American Cancer Society. Cancer facts and figures. 2004.
3. Paul B., Dhir, R. ,Landsittel, D., Hitchens M.R, and Robert H. : Detection of Prostate Cancer with a Blood-Based Assay for EarlyProstate Cancer Antigen. Cancer Research 2005, Volume 65. May 15, 2005

4. Scardino, P.T. : Early detection of prostate cancer. Urology North America, 1989 Nov; 16(4) Pages: 635-55.
5. Catalona,W.J, Smith, D.S., Ratliff, T.L: Measurement of prostate specific antigenin serum as a screening test for prostate cancer. English Journal of Medicine 1991; 324 1156-1161
6. Thompson, I.M., Pauler, D.K., Goodman, P.J. : Prelevance of prostate cancer among men with a prostate specific antigen level< or = 4.0 ng/ml" English Journal of Medicine 2004, Volume 350: 2239-2246.
7. Hoffelt, S. , Marshall, M., Garzotto, M, Hung, A., Beer, M.: A comparison of CT scan to transrectal ultrasound-measured prostate volume in untreated prostate cancer. International Journal of Radiation Oncology, volume: 57, Issue: 1, September 1, 2003, 29-32.
8. Vapnek, J.M., Hricak, H., Shinohara, K., Popovich, M., Carroll, P. : Staging accuracy of magnetic resonance imaging versus transrectal ultrasound in stages A and B prostatic cancer. Urology 1994; volume 4:191-196.
9. Smith, A.: Transrectal ultrasonography for the detection and staging of carcinoma of the prostate. Journal of Clinical Ultrasound, Volume: 24, Issue: 8, October 1996, 455 – 461.
10. Scheiper, U., Lorenz, A.: Pesavento A., Ermert, H., Sommerfeld, H., Garcia-Schurmann, M., Kuhne, K., Senge, T. and Philippou, S. :Ultrasonic multi-feature tissue characterization for the early detection of prostate cancer. IEEE Symposium on Ultrasonics, Volume: 2 , 7-10 Oct. 2001 Pages: 1265 -1268 vol.2
11. Bhanu, K.N., Ramakrishnan, A.G., Suresh, S. and Chow, T.W.P.: Fetal lung maturity analysis using ultrasound image features. IEEE Transactions on Information Technology in Biomedicine, Volume: 6 , Issue: 1 , March 2002 Pages:38 – 45
12. Chung-Ming, W., Yung-Chang, C., and Hsieh, K.: Texture features for classification of ultrasonic liver images. IEEE Transactions on Medical Imaging, Volume: 11 Issue: 2, June 1992 Pages: 141 –152
13. Feleppa, E.J., Kalisz, A., Sokil-Melgar, J.B., Lizzi, F.L., Tian, L., Rosado, A.L., Shao, M.C., Fair, W.R., Yu W., Cookson, M.S., Reuter, V.E., Heston, W.D.: Typing of prostate tissue by ultrasonic spectrum analysis. IEEE Transactions on Ultrasonics, Ferroelectrics and Frequency Control, Volume 43, Issue 4, July 1996 Page(s):609 – 619
14. Lizzi, F.L., Feleppa, E.J., Astor, M., Kalisz, A.: Statistics of ultrasonic spectral parameters for prostate and liver examinations. IEEE Transactions on Ultrasonics, Ferroelectrics and Frequency Control, Volume 44, Issue 4, July 1997 Page(s):935 – 942
15. Clausi, D.A, Jernigan, J. E.: Designing Gabor filters for optimal texture separability. Pattern Recognition Volume 33, pages: 1835-1849, 2000.
16. XX
17. Nixon, M. and Aguado, A, : Feature extraction and image processing. Newnes, 2002
18. Gonzalez, R. and Woods, R. ,: Digital Image Processing. Addison-Wesley, 1992.
19. Coggins J.M. and Jain, A.K.: A Spatial Filtering Approach to Texture Analysis. Pattern Recognition Letters, Volume 3, no. 3, Pages 195-203, 1985.
20. Randen, T.; Husoy, J.H.: Filtering for texture classification: a comparative study. IEEE Transactions on Pattern Analysis and Machine Intelligence, Volume 21, Issue 4, April 1999 Pages:291 - 310
21. Proakis, J.G., and Manolakis D.G.: Digital Signal Processing: Principles, Algorithms, and Applications. Englewood Cliffs, NJ: Prentice Hall, 1996.
22. Hayes, M.H. "Statistical Digital Signal Processing and Modeling." New York: John Wiley & Sons, 1996.
23. Gupta, I.J., Beals, M.J ,and Moghaddar, A. :Data extrapolation for high resolution radar imaging. IEEE Transactions on Antennas and Propagation , Volume 42, Issue 11, pp. 1540 – 1545, Nov. 1994

24. Vizinho A., and Wyatt L.R.: Evaluation of the use of the modified-covariance method in HF radar ocean measurement. IEEE Journal of Oceanic Engineering, Vol. 26, Issue 4, pp. 832 - 840, 2001.
25. McCoy, E.J., Walden, A.T., Percival, D.B.: Multitaper spectral estimation of power law processes
Signal Processing. IEEE Transactions on Acoustics, Speech, and Signal Processing, Volume 46, Issue 3, March 1998 :655 - 668
26. De Castro, L.N, and Von Zuben, F.J. ,: Learning and Optimization Using the Clonal Selection Principle. IEEE Transactions on Evolutionary Computation, Special Issue on Artificial Immune Systems, 6(3), pp. 239-251, 2002.
27. De Castro, L.N. and Timmis, J.I.: Artificial Immune Systems: A New Computational Intelligence Approach. Springer-Verlag, London, 2002.
28. Duda R., Hart P., Stork, D.: Pattern Classification. John Wiley and Sons.2001